

Received June 10, 2020, accepted June 12, 2020, date of publication June 16, 2020, date of current version June 30, 2020.

Digital Object Identifier 10.1109/ACCESS.2020.3002889

Adaptive Stochastic Resonance Method Based on Quantum Genetic Algorithm and Its Application in Dynamic Characteristic Identification of Bridge GNSS Monitoring Data

XINPENG WANG^{1,2}, SHENGXIANG HUANG^{1,3}, GUANQING LI^{1,2},
WEN ZHANG¹, CHENFENG LI¹, AND YARONG WANG¹

¹School of Geodesy and Geomatics, Wuhan University, Wuhan 430079, China

²Beijing Key Laboratory of Urban Spatial Information Engineering, Beijing 100038, China

³Collaborative Innovation Center of Geospatial Technology, Wuhan 430079, China

Corresponding author: Shengxiang Huang (shengxhuang@163.com)

This work was supported in part by the National Natural Science Foundation of China under Grant 41274020, and in part by the Beijing Key Laboratory of Urban Spatial Information Engineering of China under Grant 2019210.

ABSTRACT Bridge dynamic monitoring based on GNSS has become an important means of monitoring bridge structure. GNSS dynamic monitoring signals are often overwhelmed by strong noises and multipath errors. Thus the conventional data processing methods such as Fourier transform, wavelet analysis, and others have poor denoising effect or obtain unobvious dynamic characteristics from weak vibration signals. To solve this problem, the present study proposes a new adaptive stochastic resonance method based on quantum genetic algorithm with known frequency as optimal parameter. Analyzing the simulation signals not only verifies the validity and scientificity of the method, but also analyzes its frequency extraction effect in the approximate error range of target frequency with different noise intensity. A notable bridge vibration frequency is obtained when the new method is applied to analyze the bridge dynamic monitoring data based on GNSS.


INDEX TERMS Bridge dynamic characteristic identification, weak signals, adaptive stochastic resonance, quantum genetic algorithm, GNSS monitoring data.

I. INTRODUCTION

As key structures that connect railways, roads and other important facilities, bridges are vital to ensure smooth traffic and social and economic development. Due to accidents, such as the collapse of the Minnesota Bridge in the United States [1] and the Morandi Bridge in Italy [2], transportation safety has attracted close attention from governments and the public [3]. Normal operations and long-term safety of bridges are issues that cannot be overemphasized. For engineers and designers, an important research direction is continuous health monitoring and condition assessment of bridges to identify possible damage as soon as possible. Any maintenance and repair work can be implemented at the initial damage stage to maximize the life of the bridge by ensuring

the safety and reliability of the structure [4]–[7]. The material performance of bridges are degraded due to the long-term effects of wind and load or even sudden action of earthquakes and ship crash. Furthermore, the excitation of load and other environmental factors might lead to the response of the bridge [8]–[11], either healthy or with potential damage factors. Many academic and practical studies focus on monitoring and analyzing vibration frequency, velocity, acceleration, static deformation and dynamic displacement through the development of advanced sensing technology, sensors and health diagnosis methods [6], [7], [12].

A structural monitoring system needs to identify static, dynamic and permanent deformation in real time; thus researchers and engineers have developed and applied numerous monitoring tools such as intelligent total station [13]–[16], ground photogrammetry equipment [17]–[20], 3-D laser scanners [19], [21], global navigation satellite

The associate editor coordinating the review of this manuscript and approving it for publication was Jun Shen .

systems [22]–[30] and ground-based synthetic aperture radar [31]–[36] for structural deformation monitoring of bridges. These instruments, equipment and technologies have gained good monitoring achievements, but each has its own advantages and disadvantages. In particular, the first three technologies are often affected by observation distance and their monitoring accuracy is poor. Thus, many researchers have exerted efforts in updating and improvement, such as differential GNSS [26]–[28], [30], multi-frequency multi-system GNSS [38]–[42], high sampling rate [43]–[46], multi-path influence weakening [47], and denoising and filtering [48]–[51], and applied them to dynamic deformation monitoring of bridges. The advantage of continuously providing uniform 3D coordinates makes the GNSS technique increasingly popular, such that in mainland China GNSS receivers (according to incomplete statistics) have been installed in more than 30% of bridges to monitor dynamic deformation [51]. The GNSS dynamic 3D coordinate sequences obtained from the monitoring not only reflect the real-time dynamic displacement change of bridge structure but also extract frequency and modal information on bridge vibration [26]–[28], [30], [52], [53].

Since Adams *et al.* [54] proposed the concept of detecting structural damage through changes in structural natural frequencies and conducted experimental verification with his partners [55], the vibration frequencies of structures have been regarded as important modal parameters, and achievements have been made in bridge structural condition monitoring [56]–[63]. Accelerometers are often used to measure the natural frequency although scholars have different views on whether the change of bridge vibration frequency, with or without traffic load, indeed reflects the dynamic characteristic of bridge structures in a state of damage [59], [60]. The reason is that the accelerometer has some shortcomings, such as integral accumulation error, insensitivity to low-frequency vibration, and others [61]. Therefore, growing number of studies have focused on corresponding data processing methods, such as linear analysis-based methods [64], [65], wavelet transform [66]–[72], principal component analysis [73], [74], empirical mode decomposition (EMD) and its derivative method [72], [75]–[83], to extract the vibration features of bridges. Compared with difficulties in simulating and estimating the displacement error in accelerometer monitoring, a certain rule exists to address for the noise in 3D coordinate time series of bridge monitoring deformation from GNSS [84]–[87]. A growing number of researchers have adopted time series analysis methods to extract the dynamic deformation feature information on bridges through GNSS monitoring [23], [24], [30], [72], [88]–[94]. The existing methods show excellent performance in the vibration feature extraction of bridge monitoring data, but the weak vibration feature signal is seriously polluted by noise in coordinate time series. Thus, the noisy signal is denoised so blindly that it reduces the noise to a certain extent, and the characteristic signal is weakened, thereby leading to “an internecine situation”. Importantly, the gradual changes in deformation and

frequency of the bridge may be so feeble for a long time with the cumulative loading and silent material aging before failure or accident that changes of deformation or frequencies are so weak that submerged in noise of GNSS measurement. For the non-stationary time series with a large noise component or those submerged by noise, extracting the frequency significantly is difficult using conventional methods.

On another hand, stochastic resonance (SR), which was proposed by Benzi *et al.* [95] to explain the paleo-meteorological problems of glacier cycle, is different from the denoising methods mentioned, because it is a new approach to transfer noise energy to signal energy using a nonlinear system. On this basis, adaptive stochastic resonance (ASR) method developed by Mitaim and Kosko [96] can find the best balance among signal, noise and driving force, thereby generating a stochastic resonance phenomenon that can effectively detect or highlight useful signals and achieve denoising with low signal-to-noise ratio (SNR). In recent years, applications of stochastic resonance in mechanical vibration and signal noise processing have developed rapidly [97]–[103], and the effect is encouraging. However, the application to dynamic characteristic analysis of deformation coordinate time-series from GNSS monitoring on bridges is rarely reported. Thus, this study intends to analyze the time series of GNSS monitoring bridge dynamic deformation using a new adaptive stochastic resonance method to obtain more prominent bridge frequency information, which is convenient for bridge state evaluation.

II. ADAPTIVE STOCHASTIC RESONANCE BASED ON QUANTUM GENETIC ALGORITHM

A. STOCHASTIC RESONANCE THEORY

Stochastic resonance system generally consists of three factors: nonlinear system, periodic signal and noise. When the best matching relationship is achieved, the amplification effect of stochastic resonance on the signal is the most obvious [96]. The most commonly used model in the stochastic resonance study is the bistable system, which can be expressed in the nonlinear Langevin equation [95], [96]:

$$\frac{dx}{dt} = ax - bx^3 + S(t) + \xi(t), \quad (1)$$

where a , b represents non-zero system parameters, $S(t)$ is a weak periodic signal with amplitude $A \ll 1$ and $\xi(t)$ represents Gaussian white noise with zero mean, which meets the following criteria

$$E[\xi(t)\xi(t + \tau)] = 2D\delta(t - \tau). \quad (2)$$

The potential function of the above bistable system [96] is

$$V(x) = -\frac{a}{2}x^2 + \frac{b}{4}x^4. \quad (3)$$

As shown in FIGURE 1, the bistable potential function [98] has two steady states $x_{\pm} = \pm\sqrt{a/b}$, one non-steady state $x = 0$, and potential barrier height $\Delta U = a^2/4b$. When no external input exists, the system is at x_{\pm} , the lowest point of

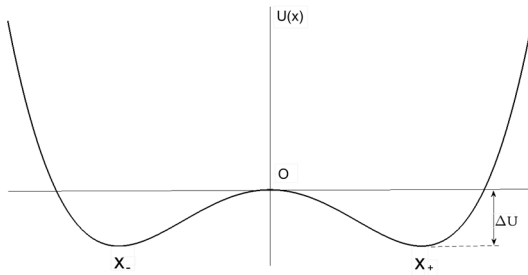


FIGURE 1. Schematic of bistable stochastic resonance system.

the potential well, where the potential energy is the smallest and the system is most stable [96]. When a weak signal $S(t)$ is added to the system, the signal energy cannot overcome the potential barrier, and the output state of the system can move in a potential well only. If the noise $\xi(t)$ is added to the system with the weak signal, the input changes into $S(t) + \xi(t)$, and then the noise energy is partially transferred to the signal, resulting in an interaction to overcome the potential barrier and a transition between the two steady states in the form of signal frequency [98]. When the potential difference between bistability is much larger than the amplitude of the input signal, the input signal is amplified, that is, stochastic resonance occurs.

In the stochastic resonance system, one of the main factors that hinder the signal transition is the potential barrier height ΔU , and the system parameters a and b together determine the value of the barrier height [96]. Therefore, the parameters a and b play a decisive role in the occurrence of stochastic resonance.

Stochastic resonance may not occur obviously when the barrier height is extremely low, and producing stochastic resonance is impossible when the barrier height is extremely large [97]. A pair of optimal parameters a and b must exist for different input signals, which can generate the best potential barrier height, and ensure occurrence of a good stochastic resonance phenomenon.

B. QUANTUM GENETIC ALGORITHM

Quantum genetic algorithm (QGA), an algorithm developed by Han and Kim [105] based on quantum basic theory and genetic algorithm thought [105], is one of the most mature quantum derivative algorithms. Subsequently, Wang et al. [106] introduced the concept of quantum rotating gate into the algorithm, which further improved the QGA. For quantum algorithms that exploit quantum mechanical features such as coherent superposition, quantum parallelism, entanglement, and measure collapse, QGA, as a global optimization algorithm, has stronger parallel computing ability than traditional algorithms [107]. QGA, with a small and fixed number of parameters, does not need adjustment according to specific practical problems, so it can be used in the self-adaptive analysis of an inversion model [108].

A bit can only express 0 or 1 in the conventional information, whereas in the quantum information, the qubit can express the superposition states of 0 and 1 at the same time, that is, any intermediate state of 0 and 1 state [105]. Therefore, the quantum may express a larger solution space with a small number of individuals, and the superposition state $|\varphi\rangle$ can be described as:

$$|\varphi\rangle = m|0\rangle + n|1\rangle, \tag{4}$$

where m, n are the probability amplitude of the corresponding qubit state, which satisfies the condition $|a|^2 + |b|^2 = 1$. The probability amplitude of qubits $|b|^2$ and $|a|^2$ tend to 0 or 1 after many iterations, that is, the quantum collapses to a definite state with the disappearance of the quantum uncertainty [105]. The expression of f -th chromosome in the chromosome population of the c -th generation is as follows:

$$X_f^c = \begin{bmatrix} a_1^c & a_2^c & \dots & a_e^c \\ b_1^c & b_2^c & \dots & b_e^c \end{bmatrix}, \quad (f = 1, 2, \dots, F), \tag{5}$$

where e is the number of qubits per chromosome and F is the number of chromosomes (chromosome population).

In QGA calculation, the variation of chromosomes in each generation is conducted by the action of the quantum gate. The probability amplitude of all qubits are rotated according to the current optimal chromosome information to improve the quantum's tendency toward the optimal solution [106]. At present, the most popularly used quantum gate is the quantum rotating gate, which has a rotation matrix of $U(\Delta\theta)$. The rotation angle $\Delta\theta$ controls the convergence speed of the algorithm, and the size and direction of $\Delta\theta$ should be determined according to the adjustment strategy table [107]. The quantum rotation gate operates as follows:

$$\begin{bmatrix} a^{c+1} \\ b^{c+1} \end{bmatrix} = U(\Delta\theta) \begin{bmatrix} a^c \\ b^c \end{bmatrix} = \begin{bmatrix} \cos(\Delta\theta) & -\sin(\Delta\theta) \\ \sin(\Delta\theta) & \cos(\Delta\theta) \end{bmatrix} \begin{bmatrix} a^c \\ b^c \end{bmatrix} \tag{6}$$

The quantum coding measurement is converted to binary coding through observation. The process of measuring collapse is as follows: a random number $rand$ is generated randomly for each quantum bit. The qubit value is 1 if $rand < |a|^2$; otherwise it is 0. Then, the binary code is transformed into a decimal system according to the variation range of independent variables of specific problems to calculate the fitness of chromosomes [107]. The flow chart of the QGA algorithm is shown in FIGURE 2.

C. ADAPTIVE STOCHASTIC RESONANCE BASED ON QUANTUM GENETIC ALGORITHM

Developing and perfecting the analytical method of adaptive stochastic resonance is necessary to extract accurate and significant bridge dynamic characteristic signals for GNSS monitoring data affected by noise. From the analysis of Section 2.1, we can find that the selection of parameters a and b of the stochastic resonance system plays an important role in its performance. However, the existing adaptive stochastic resonance methods are often optimized using genetic algorithm with two parameters as the optimization

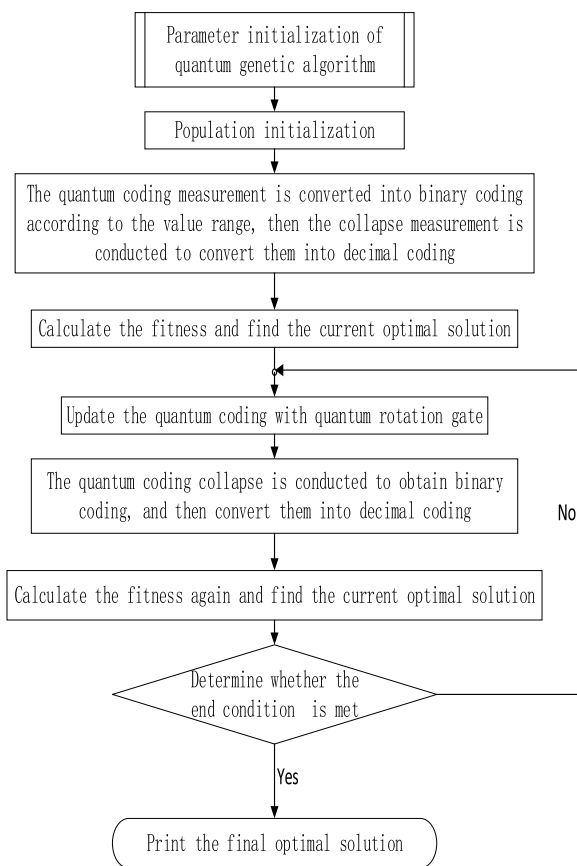


FIGURE 2. Flowchart of QGA algorithm.

object. Genetic algorithm often falls into a local optimal solution without change of other parameters when seeking the best match of stochastic resonance parameters [107]. In this study, the adaptive stochastic resonance based on quantum genetic algorithm is adopted to extract bridge vibration signal effectively and significantly, which uses the good global optimization ability of quantum genetic algorithm to realize the parallel adaptive optimization of two parameters of stochastic resonance.

According to stochastic resonance theory, the input signal must meet the requirements of small parameters (signal amplitude $A \ll 1$, noise intensity $D \ll 1$, and signal frequency $f \ll 1$). Before the parameter optimization of stochastic resonance system, the input signal, which does not meet the requirements of small parameters, has to be preprocessed through normalization, frequency shift, modulation, variable scale and frequency shift scale [105]. In this study, the frequency shift variable scale method [105] is adopted to perform the signal preprocessing, and then the adaptive stochastic resonance method based on the maximum output SNR is used to extract the vibration features.

The new adaptive stochastic resonance method uses quantum genetic algorithm to optimize the system parameters a and b of stochastic resonance simultaneously. The inverse of the SNR of the stochastic resonance output signal

is selected as the objective function value of the quantum genetic optimization algorithm, which reflects the optimization degree of the processed signal in process. The specific steps are as follows:

- (1) The parameters of quantum genetic algorithm are initialized and the fitness evaluation function of the adaptive stochastic resonance system is selected.
- (2) The frequency shift variable scale method is adopted to preprocess the input signal to meet the conditions of small parameters of stochastic resonance.
- (3) The value range of stochastic resonance system parameters a and b is determined according to the actual situation, converted into binary range, and then a set of binary parameter values is randomly generated.
- (4) The progeny chromosomes are generated by the probability of quantum gate rotation and collapse according to the parameters generated from each iteration, that is, to find the preliminary optimized system parameters a and b .
- (5) The optimized parameters are substituted into the stochastic resonance system, and then the output SNR of the input signal processed by stochastic resonance is calculated.
- (6) After many evolutions, the combination of the most optimized parameters a and b is substituted into the system to form an adaptive stochastic resonance system, and the optimization system is used to enhance and extract the weak characteristics of the signal.

III. SIMULATION EXPERIMENT ANALYSIS

To verify the objectivity and effectiveness of adaptive stochastic resonance based on quantum genetic algorithm, we conducted the following analog signal analysis.

A. ADAPTIVE STOCHASTIC RESONANCE ANALYSIS OF WEAK PERIODIC SIGNALS WITH KNOWN NATURAL FREQUENCIES

A cosine signal that meets the requirements of small parameters of stochastic resonance is simulated $S(t) = A \cos(2\pi f_0 t)$, in which the frequency and amplitude of the small parameter signal are $f_0 = 0.01\text{Hz}$, $A = 0.03$. Zero mean Gaussian white noise is added to the signal, where noise intensity is $D = 0.2$, data length is $L = 10000$, and sampling frequency is $f_s = 10\text{Hz}$. The time domain and frequency domain of the analog composite signal are shown in FIGURE 3 (A) and (B). Adaptive stochastic resonance system based on genetic algorithm (GA-ASR) and adaptive stochastic resonance system based on quantum genetic algorithm (QGA-ASR) are adopted to process the composite signal, and the parameters of the two algorithms are as follows: population number $M = 100$, evolutionary generations $MaxI = 200$, crossover probability $p_n = 0.7$, mutation probability $p_c = 0.05$, and quantum rotation probability $p_n = 0.9$. The solution accuracy of the stochastic resonance system parameters a and b is 0.001 , the fitness accuracy is 0.0001 , the value range of a is $[0.01, 200]$, and the value range of b is $[0.01, 10^4]$.

As shown in FIGURE 3 (A) and (B), the frequency of the original cosine signal is difficult to recognize on the

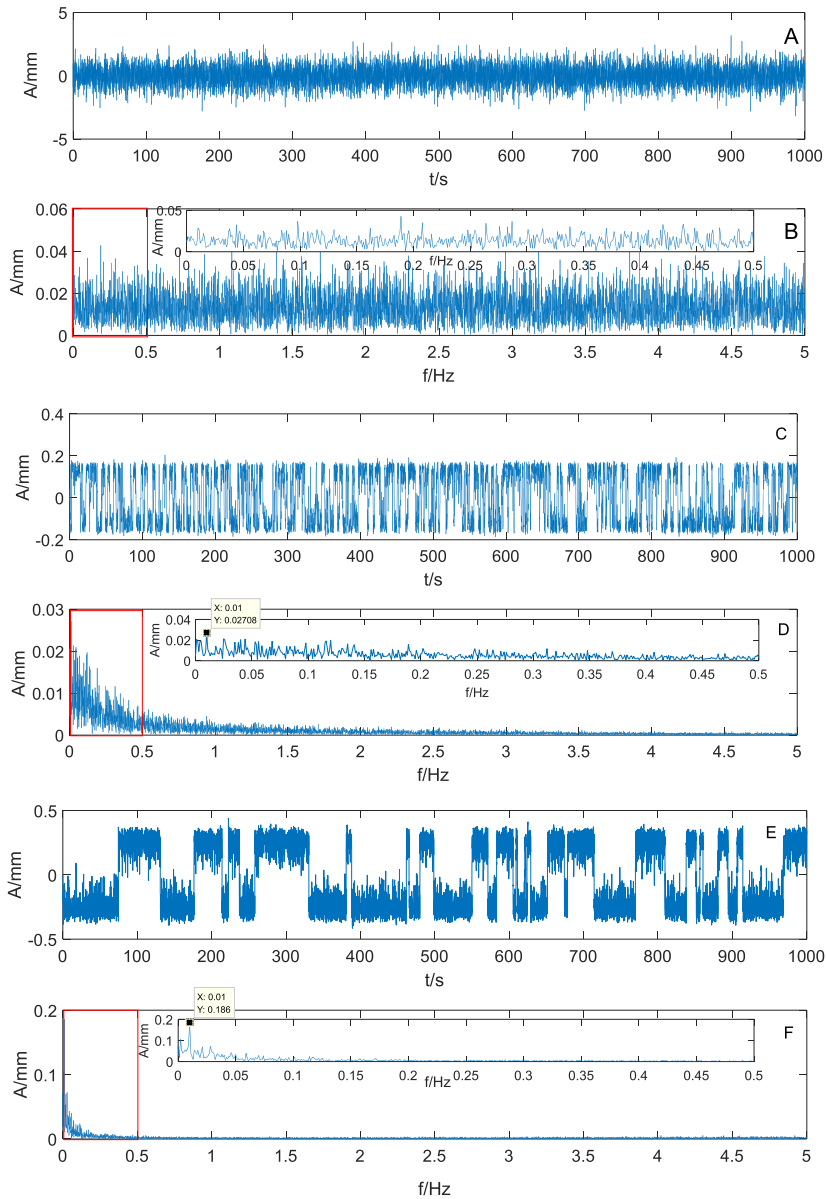


FIGURE 3. Comparison of results on weak signal detection using GA-ASR and QGA-ASR.

time-frequency diagram. After GA-ASR processing, the system parameters are calculated as $a = 7.557$, $b = 340.296$, and $SNR = -16.024$; the time and frequency diagrams are presented in FIGUR 3 (C) and (D). The Lorentz effect can be observed obviously, that is, the signal energy moves gradually towards the small frequency signal. Some small frequency band (such as 0-0.5 Hz in the red box in FIGURE 3 (D)) are redrawn as a subgraph (omitting the non-low frequency part of the signal spectrum 0.5-5 Hz) to express this effect clearly. As shown in the subgraph, the signal noise is greatly suppressed, indicating the characteristics of approximate periodic signal, which is exactly the original cosine signal. Its amplitude at the reference frequency $f_0 = 0.01Hz$ is only $A_x = 0.02708$. After QGA-ASR processing, the system parameters are calculated as $a = 17.248$, $b = 130.993$,

$SNR = -5.154$, and the time and frequency diagrams are shown in FIGURE 3 (E) and (F). As can be seen from FIGURE 3 (E), although it is not so strict and accurate, the time domain signal processed by QGA-ASR presents obvious periodic signal characteristic. Accordingly, periodism is more prominent at the frequency $f_0 = 0.01Hz$, while the domain ranges of most of the other frequencies are close to 0. We can infer that the achievement not only improves the SNR but also shows the Lorentz effect obviously. The characteristics of stochastic resonance, that is, those of periodic signals in real-time frequency maps, are more obvious and perform better in the aspect of noise removal effect. Furthermore, the amplitude of the reference frequency increases to $A_x = 0.186$, which is 6.8 times higher than that of GA-ASR. This condition greatly enhances the

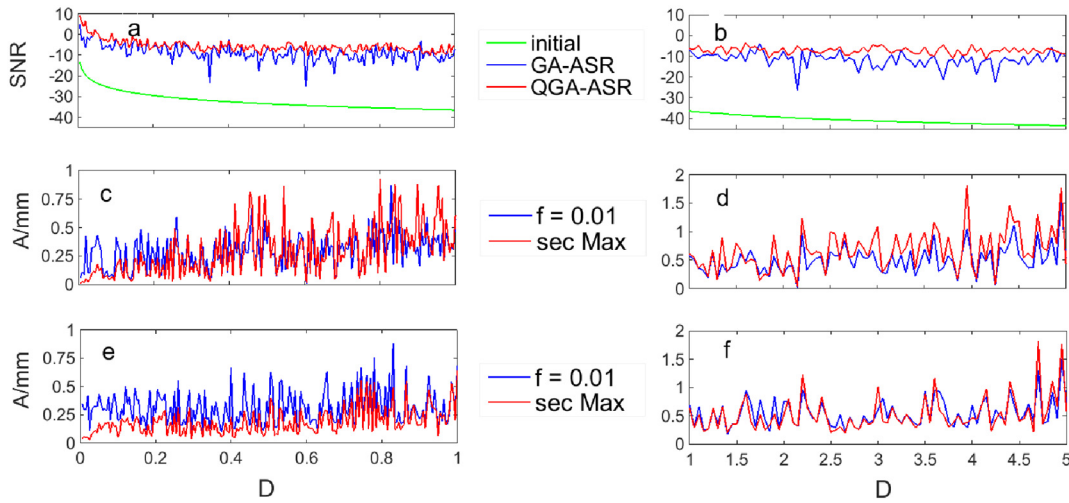


FIGURE 4. Effect analysis on detection of weak signal with different noise intensity using different ASR approaches.

periodicity of the signal and amplifies the weak signal by a large margin. Thus QGA-ASR achieves better stochastic resonance signal enhancement and Lorentz effect than that of GA-ASR due to the global optimization ability of the quantum genetic algorithm. Therefore, QGA-ASR on signal detection is highly effective, especially for weak signals.

B. ADAPTIVE STOCHASTIC RESONANCE ANALYSIS OF WEAK SIGNALS WITH DIFFERENT SNR

To examine the ability of analyzing and identifying the weak signals with different noise intensities using the QGA-ASR method, we consider a cosine signal that was the same as the parameters in section 3.1 and met the requirements of small parameters without losing its generality. Then, different degrees of zero-mean Gaussian white noise were added to the cosine signal, where noise intensity was $D_1 = 0.005 : 0.005 : 1$ and $D_2 = 1 : 0.05 : 5$. The SNRs under different noise intensities were calculated using adaptive stochastic resonance methods and system parameters, which were the same as those in section 3.1, and SNRs of the processed results by GA-ASR and QGA-ASR were abbreviated as SNR1 and SNR2, respectively, and drawn in FIGURE 4 (a) and (b). The amplitudes of $f = 0.01Hz$ obtained by GA-ASR processing the compound signal with different noise intensity are drawn in FIGURE 4 (c) by a solid blue line. While the maximum amplitudes except the frequency $f = 0.01Hz$ point of those in the frequency domain diagram are drawn by a solid red line in FIGURE 4 (d). Furthermore, the similar counterparts obtained from QGA-ASR are drawn in FIGURE 4 (e) and (f).

FIGURE 4 (a) and (b) show that although the SNR of the composite signals decrease gradually with the increase of noise intensity, it is not a strictly linear and decreasing relationship. The SNRs of the signals processed by GA-ASR and QGA-ASR have been greatly improved. Moreover, the red solid line representing the SNR of the signals processed by QGA-ASR in FIGURE 4 (a) and (b) are

above the blue solid line of the signals processed by GA-ASR in most cases, thereby indicating that the increase of QGA-ASR is more significant. On the other hand, as shown in FIGURE 4 (c) and (d), according to the representative meaning, if the red solid line is below the blue solid line, then the frequency to be detected can be detected by the method more accurately; otherwise, the frequency to be detected cannot be detected effectively. GA-ASR and QGA-ASR perform well in detection effectiveness on the initial frequency in the noise intensity range $[0, 0.2]$, as shown in FIGURE 4 (c) and (e); and in the noise intensity range $[0.2, 1]$ only QGA-ASR performs well, while a wide range of misdetection occurs in the performance of GA-ASR. As the noise intensity continues to increase, most of the red lines in the results of the GA-ASR method exceed the blue line in the noise intensity range $[1, 5]$. As shown in FIGURE 4 (d), a large-scale error detection phenomenon occurs. In the QGA-ASR method, although most of the red line does not exceed the blue line shown in FIGURE 4 (f), the two lines almost reach the same level, thereby causing difficulty in identifying the maximum value. This result indicates that bad performance of QGA-ASR occurs in the range $[1, 5]$, and an improvement in the SNR shown in FIGURE 4 (b) does not help.

To extensively compare the effectiveness of GA-ASR and QGA-ASR in detecting weak signals (only considering the noise intensity range $[0, 1]$ for the time being), we investigated the amplitude at the frequency $f = 0.01Hz$ to be detected obtained by the two methods and their amplitude enhancement relative to the maximum in the frequency domain other than the point are investigated. The distinguishable degree k_{AMP} of the amplitude of detection frequency obtained from the two methods is defined by the formula

$$k_{AMP} = \begin{cases} \frac{AMP_{f0} - AMP_{SM}}{AMP_{SM}}, & AMP_{f0} > AMP_{SM} \\ \frac{AMP_{f0} - AMP_{SM}}{AMP_{f0}}, & AMP_{f0} < AMP_{SM}, \end{cases} \quad (7)$$

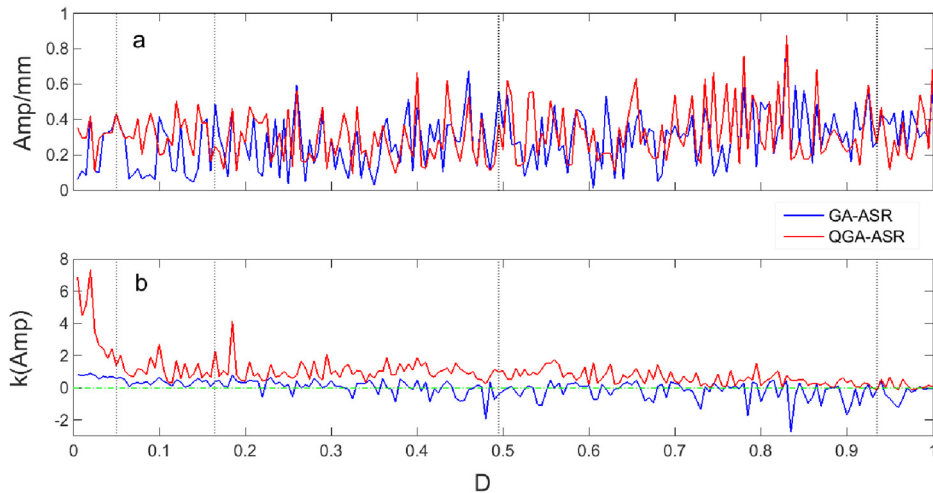


FIGURE 5. Comparison of signal enhanced extent using different ASR approaches on weak signal with different noise intensity.

where AMP_{f_0} represents the amplitude at the frequency $f = 0.01\text{Hz}$ to be detected in the frequency domain of the output signal processed by the two methods for a certain noise intensity signal, while AMP_{SM} represents the maximum amplitude except the frequency $f = 0.01\text{Hz}$ in the frequency domain (that is, the magnitude of the red solid line in FIGURE 4 (c)-(f)). Formula (7) shows that if $k > 0$, then the frequency detection is successful; if $k < 0$, then the detection fails. In particular, if k is equal to 0 or a positive number close to 0, then the detection effect is not good. To express the detail clearly, the dividing line of $k = 0$ is represented by a green dotted line, and the amplitudes of $f = 0.01\text{Hz}$ in the output frequency domain of the two methods (marked as A_{GA} and A_{QGA} respectively) are drawn in blue and red solid lines, respectively; and k_{AMP} is represented in a similar manner.

FIGURE 5 (a) shows that when the weak signals with different noise intensities are processed by the GA-ASR and QGA-ASR methods, the amplitudes of $f = 0.01\text{Hz}$ in the frequency domain of the two methods exceed each other, but this approach cannot determine which is better or worse. We can infer from FIGURE 5 (b), that the distinguishable degree (marked as k_{QGA}) of the frequency to be detected after the QGA-ASR process is significantly better than that (marked as k_{GA}) of GA-ASR. However, among the amplitudes of $f = 0.01\text{Hz}$ in the frequency domain of FIGURE 5 (a), there are cases in which A_{GA} is larger than A_{QGA} , such as where $D = 0.165$; there are cases in which k_{GA} is smaller than k_{QGA} among the distinguishable degree of FIGURE 5 (b) especially correspondingly to $D = 0.165$; or even cases where A_{GA} is close to A_{QGA} such as where $D = 0.5$, there are cases in which k_{GA} is approaching k_{QGA} . In particular, a considerable range of noise intensity exists such as $D = 0.495$, and the case of $k_{GA} < 0$ exists correspondingly, which indicates an error in frequency detection. As these experiments are conducted independently, a different white noise is generated each time to form an

analog signal. Thus, different experiments produce different processing results. Therefore, the preceding analysis and results can be regarded as universal and repeatable. In general, the optimization ability of QGA is better than that of GA, so the frequency detection effect of QGA-ASR is better than that of GA-ASR in most cases; except for a slight noise intensity, the former is at least equal to the latter. Furthermore, the k obtained by the two methods is less than 0 when the noise intensity $D = 0.945$, which needs further analysis.

C. ADAPTIVE STOCHASTIC RESONANCE ANALYSIS OF NOISE SIGNALS

The frequency detection error of the GA-ASR and QGA-ASR process of the signal with the noise intensity $D = 0.945$ in section 3.2, may be related to the high noise intensity. The reason may be that the amplitude of $f_0 = 0.01\text{Hz}$ in the output frequency domain obtained from the two methods cannot exceed the maximum amplitude among the frequency domain except the point under most cases with different noise intensities in FIGURE 4 (d) and (f). The similar simulation data with section 3.2 were used to verify this conjecture, and the only difference is the noise added to the cosine signal, where only independent tests of $D = 1$, $D = 2$, $D = 3$ and $D = 4$ are conducted for 10 times, respectively. In this case, the noise intensity is much higher than that in the 3.2 section test; such a test signal is regarded as very weak in this study. The same methods with section 3.2 were adopted to process the analog composite signals, and the results of the four independent tests are presented in FIGURE 6 (a)-(d). In view of the fact that each of the four groups has been tested 10 times, the distinguishable degree k of GA-ASR and QGA-ASR is drawn in the blue and red pentagrams, respectively.

For the very weak signals with the same noise intensity whose noise composition are from 10 different experiments, each amplitude distinguishable degree k in the results processed by the ASR method is different from the results

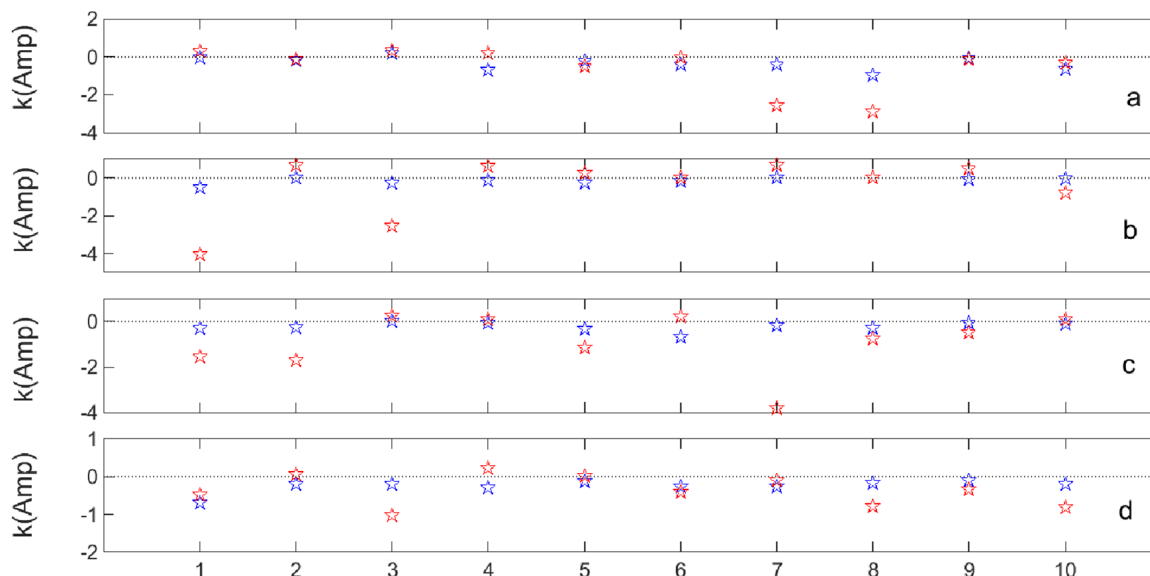


FIGURE 6. Effect analysis on extremely weak signal using different ASR approaches.

processed by ASR method is different from others because the random white noise is generated independently. When D is 1, 2, 3 and 4 respectively, even if the frequency detection effect of QGA-ASR is better than that of GA-ASR, k is close to 0 or less than 0 in many tests, which means that these frequency detection results are wrong. If we heighten noise intensity D further and perform many experiments, then the times of frequency detection errors will also increase with the heightener of D . All the test frequency detections may fail, even for QGA-ASR with better weak signal detection ability when the noise intensity D is large enough. Therefore, the ratio of noise intensity D (or the maximum amplitude of noise $\sqrt{2D}$ calculated using formula (2)) to the amplitude of signal $A = 0.03$ is larger with the continuous heightener of D , and the frequency detection test on the extremely weak signal also fails.

A zero-mean Gaussian white noise is simulated by *Matlab 2014b* to verify the aforementioned conjecture, whose noise intensity is $D = 0.2$, the data length is $L = 10000$, and the sampling frequency is $f_s = 10Hz$. The analog signal is analyzed by the same methods shown in section 3.1, where $f_0 = 0.01Hz$ is considered as the target frequency (in fact, the frequency does not exist in the weak signal) in the ASR process. The analysis results of the time and frequency domain are drawn in FIGURE 7, where only the 0-0.5 Hz frequency range diagram is drawn to compare clearly with the analysis results of “the very weak signal”.

The time and frequency diagrams of the original signal in FIGURE 7 (A) and (B) are as the same as those presented in FIGURE 3 (A) and (B), and any frequency is difficult to recognize. After the same GA-ASR process, FIGURE 7 (C) and (D) seem to show a certain Lorentz effect, but the frequency $f_x = 0.005Hz$ is not consistent with the reality, that is, not only is there no such frequency in the

white noise signal, but the frequency is also different from the assumed target frequency. Similarly, the $f_x = 0.002Hz$ in FIGURE 7 (E) (F) obtained from QGA-ASR processing is also inconsistent with reality. This shows that the bistable stochastic resonance system cannot extract or detect the “weak signal” from the pure white noise, and is ineffective when used with the QGA-ASR method, which possesses better global solution search performance. These experimental results show that the weak signal detection of adaptive stochastic resonance system is not “achieved randomly”, but through scientific and effective processes.

D. ADAPTIVE STOCHASTIC RESONANCE ANALYSIS OF WEAK PERIODIC SIGNAL WITH WRONG NATURAL FREQUENCY

In practical engineering, sometimes determining the exact frequency of a signal to be detected is difficult and only the approximate frequency can be inferred. A cosine signal $S(t) = A \cos(2\pi f_0 t)$ is simulated to investigate the frequency detection effect in the case where the approximate target frequency is known, which meets the requirements of small parameters. The frequency of the small parameter signal is $f_0 = 0.01Hz$, the amplitude $A = 0.03$, the data length is $L = 10000$ and the sampling frequency is $f_s = 5Hz$. The zero-mean-value Gaussian white noise with different intensity are added to the cosine signal, where the noise intensities is $D = 0.05 : 0.05 : 1$ in turn, which constitutes the weak signal submerged by different noise intensity. Methods similar to those discussed in section 3.2 are adopted to analyze the signal sequences one by one with regard to different frequencies $f_{0s} = 0.0093 : 0.0001 : 0.0107 (Hz)$ as the target frequencies in this study.

Different noise intensity D is regarded as x -axis, different target frequency f is used as y -axis, and the amplitude

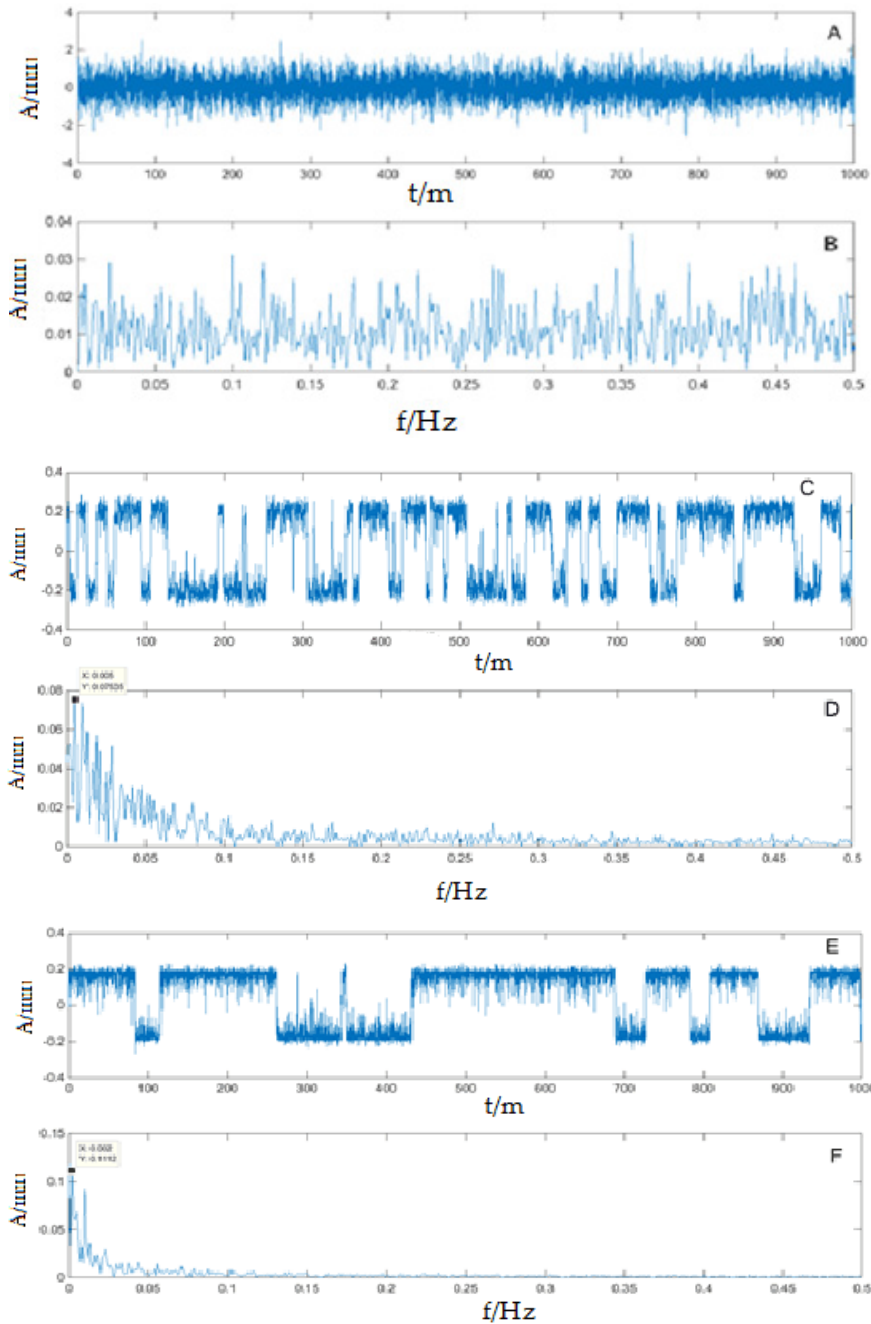


FIGURE 7. Comparison of results on noise signal detection using GA-ASR and QGA-ASR.

distinguishable degrees k_{GA} and k_{QGA} of the frequency to be detected obtained from different weak signals processed by GA-ASR and QGA-ASR based on different frequency f are taken as z-axis and drawn in the form of a stereogram in FIGURE 8. In the graph, we not only draw the case where k changes among the variations of f and D but also draw the thin sheet at $k = 0$ (in yellow color) to clearly distinguish the positive and negative k values. We can observe from FIGURE 8 that the analysis results of the two methods show k value less than 0 in a certain range of the target

frequency f , and both of them can detect the target frequency in a certain neighborhood close to the correct target frequency $f_0 = 0.01Hz$. In particular, a larger range exists in which the amplitude distinguishable degree obtained by QGA-ASR is larger than 0, compared with that of GA-ASR.

The results shown in FIGURE 8 are transferred to a plane in FIGURE 9 to further clarify the specific range of the frequency to be detected successfully. Analogously, to better distinguish the positive and negative value of k , it is preprocessed as follows: if $k > 0$, then 2 is added to the

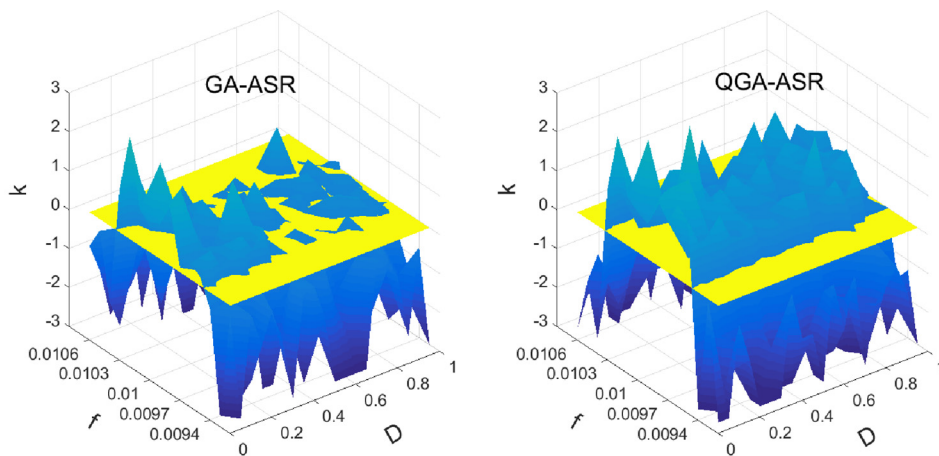


FIGURE 8. Stereogram of effect analysis on weak signal with different noise intensity using different ASR approaches based on different target frequency.

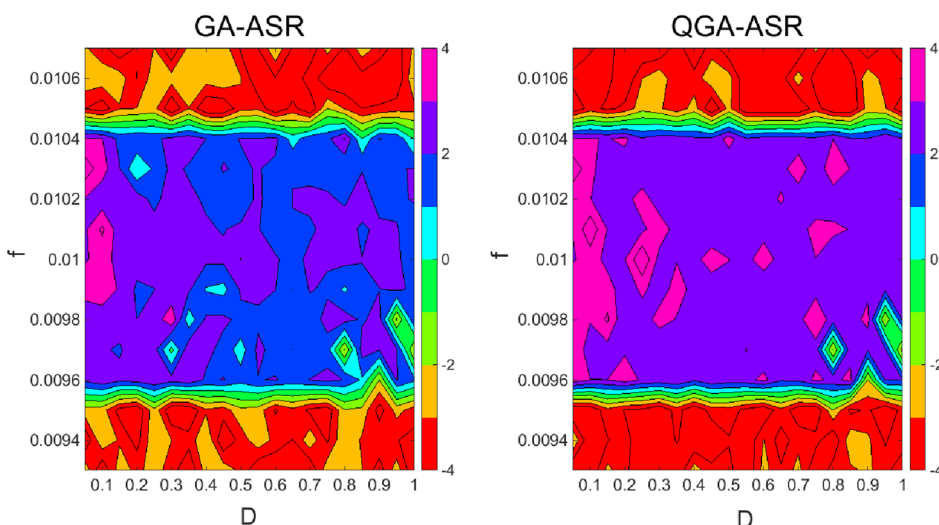


FIGURE 9. Plane of effect analysis on weak signal with different noise intensity using different ASR approaches based on different target frequencies.

value of k ; otherwise, if $k < 0$, then 2 is subtracted. We can observe in the plane diagram that when the frequency section $[0.0096, 0.0104]$ is regarded as the target frequency range to analyze the weak signal, both methods can obtain a high success rate in frequency detection; however, each method can hardly obtain a high success rate in the target frequency range of $[0.0093, 0.0096]$ and $[0.104, 0.0107]$, which are outside the above range. Moreover, in the frequency range $[0.0096, 0.0104]$, there are more amplitude distinguishable degrees k_{QGA} (the value has been subtracted from 2, which is similarly done hereafter) obtained from the QGA-ASR method larger than 3 (the magenta area is larger); in most of the frequency ranges the amplitude distinguishable degrees k_{QGA} exceed 1 (light blue region). However, in the frequency range adjacent to $[0.8, 0.95]$ and $f = 0.0096$ Hz, the amplitude distinguishable degrees obtained from the two methods are all less than 0, which means that misdetection may occur if

the approximate target frequency is slightly different from the real frequency when the signal is extremely weak. On the other hand, the SNR extreme value (calculated by the approximate target frequency) optimized in the process of adaptive stochastic resonance, is also considerably different from the actual SNR (calculated by the true frequency of the signal), with the increase of the difference between the approximate target frequency and the real frequency of the signal. This condition also verifies the importance of determining the true frequency of the signal in advance. Due to space limitations, the different SNRs are not reported in this study.

We can sum up that QGA-ASR can detect the frequency characteristics of weak signal clearly and suppress noise effectively through the aforementioned analysis. This approach works well even for the detection of the approximate frequency, where a small difference from the actual frequency is regarded as target frequency. Moreover, for the

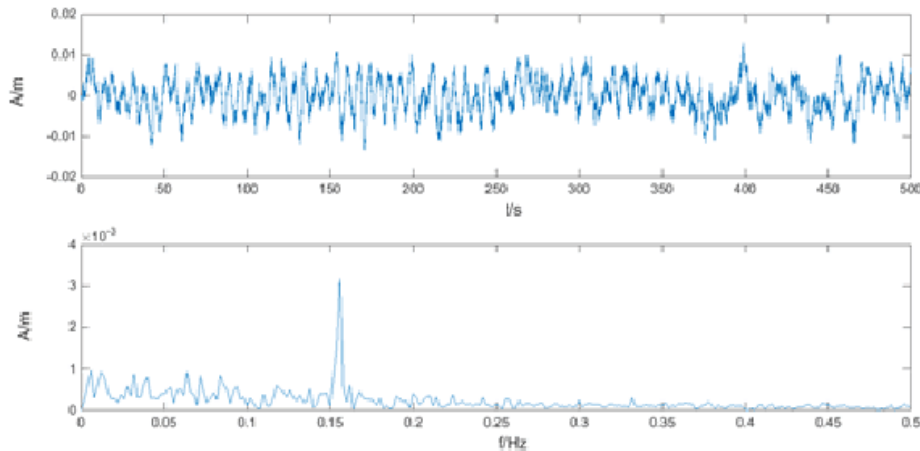


FIGURE 10. Time and frequency graph of dynamic monitoring signals of bridge using GNSS.

extremely noisy signal (neither it does not contain any specific meaningful signal, or the scale of the weak signal is too small and it falls alone to this category let alone), the two ASR methods cannot detect its right frequency; for the frequency detection that a large difference between the actual frequency and target frequency, frequency misdetection always occurs regardless of the ASR methods adopted.

IV. ENGINEERING APPLICATION

In this study, the QGA-ASR method is applied to the analysis of GNSS monitoring data of bridges.

A. ENGINEERING DATA SOURCES

Sutong Yangtze River Highway Bridge, commonly known as Sutong Bridge, is located between the cities of Nantong and Suzhou in eastern Jiangsu Province. The bridge is a double-tower and double-plane steel box girder cable-stayed structure with a total length of 8146 m, a main span of 1088 m and a main cable tower of 300.4 m high. The bridge located downstream of the Yangtze River is often hit by typhoons in the summer every year. Various bad factors, coupled with the temperature difference between day and night and seasonal variation, have a very adverse impact on the accurate positioning of the superstructure of the cable tower. High requirements are proposed to determine geometric line type, elevation, dynamic parameters, and cable tower deviation of the main beam to ensure the construction safety and index of bridge structure design during the construction period. A set of remote real-time dynamic geometric monitoring system based on GNSS technology had been established, which can monitor the geometry and structural state of towers and beams continuously and in real-time [25]. The GNSS monitoring equipment was installed on top of the cable tower as soon as the roof was sealed. For the natural frequency of the large cable-stayed bridge that is generally much less than 5 Hz, the vibration signal can be recorded by setting the sampling rate of the GNSS receiver at the monitoring point to 10 Hz

according to the Nyquist theorem, which provides a scientific basis for the safe construction of the bridge [25].

The GNSS system used Kalman filter and double difference solution algorithm to process the measurement data, and a real-time displacement result with high accuracy can be obtained [23], [24]. The bridge GNSS monitoring data series was transformed into the bridge axis coordinate system, and then averaged, and the accuracy of the data sequence is surveyed. The plane accuracy is $\delta_x = 3.6\text{mm}$, and $\delta_y = 2.8\text{mm}$, which is better than that of $\pm 5\text{mm}$, thereby indicating that it enables dynamic characteristic analysis of bridges.

B. APPLICATION ANALYSIS

We analyzed a section of x-direction monitoring time series data starting at 20:32 on December 26, 2006, with a duration of 500 s. The data were collected from the GNSS monitoring point in the bridge axis coordinate system on the north bridge tower. The time and frequency domains are drawn in FIGURE 10. The frequency domain obtained by FFT method has an obvious frequency signal $f = 0.156\text{Hz}$, but the frequency domain extreme value is small at an order of magnitude of 10^{-3} mm. Furthermore, a certain influence of noise exists.

To meet the condition of stochastic resonance and its small parameters, we apply the quadratic spline curve fitting method to make the frequency domain of the signal distributed symmetrically around 0, and then we analyze the signal through the combination of heterodyne spectrum analysis and stochastic resonance principle [109]. The ideal of the heterodyne spectrum analysis [109] is as follows: the known signal $f_c = 0.152\text{Hz}$ is multiplied by the original signal $s(t) = A_0 \cos(2\pi f_0 t) + n(t)$ (the difference of frequency between the two signals is 0.004 Hz); for $\cos(2\pi f_0 t) \cdot \cos(2\pi f_c t) = \frac{1}{2} [\cos(2\pi(f_0 - f_c)t) + \cos(2\pi(f_0 + f_c)t)]$, two signals with frequencies of $f_0 \pm f_c$ can be obtained. The signal $f_0 + f_c$ converts the energy to the $f_0 - f_c$ with lower frequency due to the stochastic resonance effect if $f_0 + f_c \geq f_0 - f_c$ exists.

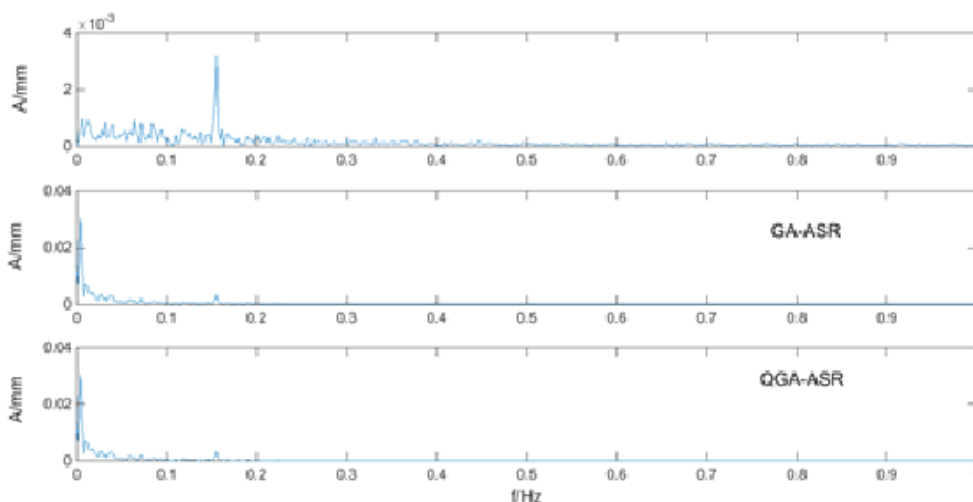


FIGURE 11. Frequency domain graphs obtained from different methods on dynamic monitoring signals of bridge using GNSS.

Then the heterodyne signal is processed by GA-ASR and QGA-ASR methods, respectively, where $f_0 - f_c = 0.005\text{Hz}$ is regarded as the extreme value objective function of SNR, and the selection of other parameters is same as that in section 3.1. Stochastic resonance occurs through the GA-ASR method when the system structural parameters a and b are 0.135 and 126.833 respectively, and the maximum value obtained is $SNR = -2.118$. Stochastic resonance occurs through the QGA-ASR method when the parameters a and b are 0.028 and 15.636, respectively, and the maximum value obtained is $SNR = -0.656$. The spectrum diagrams obtained from the two algorithms are drawn in FIGURE 11, and the spectrum obtained by FFT transform of the heterodyne signal is also drawn in the diagram for comparison.

We can infer from the diagram that the spectral peak of $f = 0.004\text{Hz}$ obtained from the GA-ASR and QGA-ASR methods, which corresponds to 0.156 Hz in the original signal according to the heterodyne method, is consistent with the preset vibration frequency of the bridge tower. We prove that the tower of the bridge is in a safe state during this period. The amplitudes of the spectral peak A in the latter two pictures reach both 3.06×10^{-2} , which is nearly 10 times higher than the 3.17×10^{-3} obtained by simple usage of FFT. This condition makes the vibration frequency signal more significant.

The amplitudes of the peaks obtained by the GA-ASR and QGA-ASR methods shown in FIGURE 11 are the same, which indicates that the optimization ability of GA and QGA is the same. These results are consistent with the analysis in section 3.3 that “the weak signal detection of the two algorithms is the same under partial noise intensity”. On the other hand, even if $f_0 - f_c = 0.005\text{Hz}$ is regarded as the extreme objective function of SNR (this is not consistent with the reality where the actual situation is $f_0 - f_c = 0.004\text{Hz}$)

in the ASR process, the final spectral peak can still fall at 0.004 Hz. This result is another strong evidence that the analysis of section 3.4 is correct and scientific. However, a smaller spectral peak also exists at the 0.156Hz in the last two subgraphs, which is the frequency of the original signal. This situation may be related to the imperfection of the Lorentz effect, or the fact that the gap between $f_0 \pm f_c$ is not large enough.

In addition, the damage identification method proposed by Rytter according to the damage state of the bridge is defined by the following levels: (i) detecting the existence of damage, (ii) determining the location of damage, (iii) estimating the degree of damage, and (iv) determining the effect of damage and predicting the remaining fatigue life.

This method can be used to monitor and detect the weak characteristic change of the structure submerged in noise from the time series of GNSS dynamic monitoring during the construction and operation of the bridge, when the bridge tower and other structures are relatively geometrically stable and the vibration characteristics are obvious. To achieve the goal of level (i), we can use this method in the cases where relative geometry of bridge towers and other structures is stable during bridge construction and operation from the time series of GNSS dynamic monitoring, and the vibration characteristics exist but is not very significant. From the time series of GNSS dynamic monitoring of the bridge, the weak characteristics and slight changes of the structure submerged in noise can be monitored and detected using the new method. The unfavorable situation is grasped in advance to achieve the goal of level (i). Based on the application range of this method and the physical structure of the relatively stable bridge structure, for example, from 0.154 Hz to 0.156 Hz, the “fault” level in the field of mechanical engineering is not yet reached, and thus the term “fault signal detection” is unsuitable. A reasonable term is “vibration frequency change

monitoring”, which is closely related to the early detection of damage of the level (i) bridge structure, and has important practical application value.

Finally, the proposed algorithm has high computational complexity and is unsuitable for the rapid characteristic identification and analysis of bridge dynamic monitoring data based on GNSS in the case of sudden mode changes. Focusing on the global optimization ability of quantum genetic algorithm, thereby improving the accuracy and prominent detection of frequency and its subtle changes, the QGA-ASR method does not consider the computational complexity reducing like the discussion in [111], thus it is as time-consuming as GA-ASR. This method also does not consider the bridge dynamic characteristic identification and signal denoising described in [94] and [112], which can be conducted in a situation where the noise amplitude is not large and the approximate frequency is unknown. However, in analyzing the bridge health monitoring data, QGA-ASR has a better ability than GA-ASR to identify or examine the frequency in the normal operation stage of the bridge. This task involves detecting the main vibration frequency and its slight changes on the bridge using the QGA-ASR method when the dynamic deformation is small or the main vibration frequency is submerged in the noise under various environmental excitations. Complementary analysis and identifying possible damage in advance are necessary so that measures can be taken to protect the bridge structure. Acting early on potential damage to the bridge is possible when a large irregular mutation in dynamic deformation or the main vibration frequency of the structure is monitored. With regard to the scientific judgment on whether the main vibration frequency of the bridge changes before and after the weak external environment varies, this method has an advantage but at the cost of high calculation complexity and time spent on identifying the weak frequency and its slight changes prominently. Therefore, it is worthwhile to use such a relatively time-consuming algorithm to identify possible damage of the bridge in the early stage.

V. CONCLUSION

In this paper, a parameter optimization adaptive stochastic resonance algorithm based on quantum genetic algorithm is proposed. The SNR of the bistable system output was regarded as the fitness function, and the quantum genetic algorithm was used to optimize the global optimization ability. The structural parameters of the stochastic resonance system were optimized to accomplish the extraction of the periodic components of the weak periodic signal in the analog signal.

According to the simulation experiment, the QGA-ASR method was validated to perform better than the GA-ASR method in dealing with the weak signal with different SNR. Stochastic resonance was not observed in the pure white signal without any weak signal. Furthermore, the QGA-ASR method was verified to be superior to the GA-ASR method when SNR was used as the fitness function to optimize the

structural parameters for the frequency detection in which the approximate frequency had a small difference from the actual frequency that was regarded as target frequency.

With the combination of heterodyne and QGA-ASR method, the vibration signal of bridge dynamic monitoring based on GNSS was extracted successfully under the condition of large parameters. Although this method did not consider the special cases, such as irregular vibration signals and non-white noise signals, in GNSS bridge monitoring, and was slightly more time-consuming, it had a significant feature extraction effect in the case of approximate frequency of vibration is known and was inundated by white noise. However, the method had a good engineering application value in finding the early abnormal changes that occurred on bridges as a result of vibration.

REFERENCES

- [1] *Highway Accident Report: Collapse of I-35w Highway Bridge Minneapolis, Minnesota August 1 2007*, House Representatives, Minneapolis, MN, USA, 2008.
- [2] H. Fountain, “In Italy Bridge Collapse, Both Design and Upkeep Are Under Suspicion,” *New York Times*, 2018. [Online]. Available: <https://www.nytimes.com/2018/08/16/world/europe/italy-bridge-collapse-design.html>
- [3] S. M. Khan, S. Atamturktur, M. Chowdhury, and M. Rahman, “Integration of structural health monitoring and intelligent transportation systems for bridge condition assessment: Current status and future direction,” *IEEE Trans. Intell. Transp. Syst.*, vol. 17, no. 8, pp. 2107–2122, Aug. 2016.
- [4] Y. J. Yan, L. Cheng, Z. Y. Wu, and L. H. Yam, “Development in vibration-based structural damage detection technique,” *Mech. Syst. Signal Process.*, vol. 21, no. 5, pp. 2198–2211, Jul. 2007.
- [5] W. Fan and P. Qiao, “Vibration-based damage identification methods: A review and comparative study,” *Struct. Health Monit. Int. J.*, vol. 10, no. 1, pp. 83–111, Jan. 2011.
- [6] J. P. Amezcua-Sanchez and H. Adeli, “Signal processing techniques for vibration-based health monitoring of smart structures,” *Arch. Comput. Methods Eng.*, vol. 23, no. 1, pp. 1–15, Mar. 2016.
- [7] D. Goyal and B. S. Pabla, “The vibration monitoring methods and signal processing techniques for structural health monitoring: A review,” *Arch. Comput. Methods Eng.*, vol. 23, no. 4, pp. 585–594, Dec. 2016.
- [8] J. J. Moughty and J. R. Casas, “A state of the art review of modal-based damage detection in bridges: Development, challenges, and solutions,” *Appl. Sci.*, vol. 7, no. 5, p. 510, May 2017.
- [9] Y. B. Yang and J. P. Yang, “State-of-the-art review on modal identification and damage detection of bridges by moving test vehicles,” *Int. J. Struct. Stability Dyn.*, vol. 18, no. 2, Feb. 2018, Art. no. 1850025.
- [10] H. He, W. Wang, and X. Zhang, “Frequency modification of continuous beam bridge based on co-integration analysis considering the effect of temperature and humidity,” *Struct. Health Monitor.*, vol. 18, no. 2, pp. 376–389, Mar. 2019, doi: [10.1177/1475921718755573](https://doi.org/10.1177/1475921718755573).
- [11] M. P. Limongelli, “Frequency response function interpolation for damage detection under changing environment,” *Mech. Syst. Signal Process.*, vol. 24, no. 8, pp. 2898–2913, Nov. 2010.
- [12] J. Ou and H. Li, “Structural health monitoring in mainland China: Review and future trends,” *Struct. Health Monit. Int. J.*, vol. 9, no. 3, pp. 219–231, May 2010.
- [13] P. A. Psimoulis and S. C. Stiros, “Measurement of deflections and of oscillation frequencies of engineering structures using robotic theodolites (RTS),” *Eng. Struct.*, vol. 29, no. 12, pp. 3312–3324, Dec. 2007.
- [14] P. A. Psimoulis and S. C. Stiros, “Experimental assessment of the accuracy of GPS and RTS for the determination of the parameters of oscillation of major structures,” *Comput.-Aided Civil Infrastruct. Eng.*, vol. 23, no. 5, pp. 389–403, Jul. 2008.
- [15] E. J. Cross, K. Y. Koo, J. M. W. Brownjohn, and K. Worden, “Long-term monitoring and data analysis of the Tamar bridge,” *Mech. Syst. Signal Process.*, vol. 35, nos. 1–2, pp. 16–34, Feb. 2013.

- [16] P. A. Psimoulis and S. C. Stiros, "Measuring deflections of a short-span railway bridge using a robotic total station," *J. Bridge Eng.*, vol. 18, no. 2, pp. 182–185, Feb. 2013.
- [17] H. Erdoğan and E. Güllal, "Ambient vibration measurements of the bosphorus suspension bridge by total station and GPS," *Experim. Techn.*, vol. 37, no. 3, pp. 16–23, May 2013.
- [18] D. V. Jáuregui, K. R. White, C. B. Woodward, and K. R. Leitch, "Non-contact photogrammetric measurement of vertical bridge deflection," *J. Bridge Eng.*, vol. 8, no. 4, pp. 212–222, Jul. 2003.
- [19] M. R. Jahanshahi and S. F. Masri, "A new methodology for non-contact accurate crack width measurement through photogrammetry for automated structural safety evaluation," *Smart Mater. Struct.*, vol. 22, no. 3, Mar. 2013, Art. no. 035019.
- [20] B. Riveiro, H. González-Jorge, M. Varela, and D. V. Jauregui, "Validation of terrestrial laser scanning and photogrammetry techniques for the measurement of vertical underclearance and beam geometry in structural inspection of bridges," *Measurement*, vol. 46, no. 1, pp. 784–794, Jan. 2013.
- [21] X. Zhao, H. Liu, Y. Yu, X. Xu, W. Hu, M. Li, and J. Ou, "Bridge displacement monitoring method based on laser projection-sensing technology," *Sensors*, vol. 15, no. 4, pp. 8444–8463, Apr. 2015.
- [22] H. S. Park, H. M. Lee, H. Adeli, and I. Lee, "A new approach for health monitoring of structures: Terrestrial laser scanning," *Comput.-Aided Civil Infrastruct. Eng.*, vol. 22, no. 1, pp. 19–30, Jan. 2007.
- [23] L. Xu, J. J. Guo, and J. J. Jiang, "Time–frequency analysis of a suspension bridge based on GPS," *J. Sound Vib.*, vol. 254, no. 1, pp. 105–116, Jun. 2002.
- [24] S. X. Huang, X. Liu, Y. B. Yang, and Y. Zhang, "Experiment and result for measuring dynamic characteristics of large bridge using GPS," *Geomatics Inf. Sci. Wuhan Univ.*, vol. 29, no. 3, pp. 198–200, 2004.
- [25] S. X. Huang, B. C. Yang, and X. P. You, "Applications of GPS dynamic geometric deformation monitoring system to Sutong Bridge," *Geomatics Inf. Sci. Wuhan Univ.*, vol. 34, no. 9, pp. 1072–1075, 2009.
- [26] X. Meng, G. W. Roberts, A. H. Dodson, E. Cosser, J. Barnes, and C. Rizos, "Impact of GPS satellite and pseudolite geometry on structural deformation monitoring: Analytical and empirical studies," *J. Geodesy*, vol. 77, no. 12, pp. 809–822, Jun. 2004.
- [27] X. Meng, A. H. Dodson, G. W. Roberts, and M. Andreotti, "Prototype Internet RTK GPS for bridge deformation monitoring," *Surv. Rev.*, vol. 38, no. 299, pp. 348–357, Jan. 2006.
- [28] M. T. Elnabwy, M. R. Kaloop, and E. Elbeltagi, "Talkha steel highway bridge monitoring and movement identification using RTK-GPS technique," *Measurement*, vol. 46, no. 10, pp. 4282–4292, Dec. 2013.
- [29] S. B. Im, S. Hurlbaus, and Y. J. Kang, "Summary review of GPS technology for structural health monitoring," *J. Struct. Eng.*, vol. 139, no. 10, pp. 1653–1664, Oct. 2013.
- [30] J. Yu, B. Yan, X. Meng, X. Shao, and H. Ye, "Measurement of bridge dynamic responses using network-based real-time kinematic GNSS technique," *J. Surveying Eng.*, vol. 142, no. 3, Aug. 2016, Art. no. 04015013.
- [31] M. Pieraccini, M. Fratini, F. Parrini, C. Atzeni, and G. Bartoli, "Interferometric radar vs. accelerometer for dynamic monitoring of large structures: An experimental comparison," *NDT E Int.*, vol. 41, no. 4, pp. 258–264, Jun. 2008.
- [32] C. Gentile, "Deflection measurement on vibrating stay cables by non-contact microwave interferometer," *NDT E Int.*, vol. 43, no. 3, pp. 231–240, Apr. 2010.
- [33] C. Gentile and G. Bernardini, "Radar-based measurement of deflections on bridges and large structures," *Eur. J. Environ. Civil Eng.*, vol. 14, no. 4, pp. 495–516, Apr. 2010.
- [34] S. X. Huang, L. Luo, and C. He, "Comparative test analysis for determining bridge deflection by using ground-based SAR and GPS," *Geomatics Inf. Sci. Wuhan Univ.*, vol. 37, no. 10, pp. 1173–1176, 2012.
- [35] C. Negulescu, G. Luzi, M. Crosetto, D. Raucoules, A. Roullé, D. Monfort, L. Pujades, B. Colas, and T. Dewez, "Comparison of seismometer and radar measurements for the modal identification of civil engineering structures," *Eng. Struct.*, vol. 51, no. 2, pp. 10–22, Jun. 2013.
- [36] O. Monserrat, M. Crosetto, and G. Luzi, "A review of ground-based SAR interferometry for deformation measurement," *ISPRS J. Photogramm. Remote Sens.*, vol. 93, no. 7, pp. 40–48, Jul. 2014.
- [37] X. Liu, X. Tong, K. Ding, X. Zhao, L. Zhu, and X. Zhang, "Measurement of long-term periodic and dynamic deflection of the long-span railway bridge using microwave interferometry," *IEEE J. Sel. Topics Appl. Earth Observ. Remote Sens.*, vol. 8, no. 9, pp. 4531–4538, Sep. 2015.
- [38] J. Yu, X. Meng, X. Shao, B. Yan, and L. Yang, "Identification of dynamic displacements and modal frequencies of a medium-span suspension bridge using multimode GNSS processing," *Eng. Struct.*, vol. 81, pp. 432–443, Dec. 2014.
- [39] R. Xi, W. Jiang, X. Meng, H. Chen, and Q. Chen, "Bridge monitoring using BDS-RTK and GPS-RTK techniques," *Measurement*, vol. 120, pp. 128–139, May 2018.
- [40] R. Xi, X. Meng, W. Jiang, X. An, and Q. Chen, "GPS/GLONASS carrier phase elevation-dependent stochastic modelling estimation and its application in bridge monitoring," *Adv. Space Res.*, vol. 62, no. 9, pp. 2566–2585, Nov. 2018.
- [41] R. Xi, W. Jiang, X. Meng, X. Zhou, and Q. He, "Rapid initialization method in real-time deformation monitoring of bridges with triple-frequency BDS and GPS measurements," *Adv. Space Res.*, vol. 62, no. 5, pp. 976–989, Sep. 2018.
- [42] R. Xi, H. Chen, X. Meng, W. Jiang, and Q. Chen, "Reliable dynamic monitoring of bridges with integrated GPS and BeiDou," *J. Surveying Eng.*, vol. 144, no. 4, Nov. 2018, Art. no. 04018008.
- [43] T.-H. Yi, H.-N. Li, and M. Gu, "Experimental assessment of high-rate GPS receivers for deformation monitoring of bridge," *Measurement*, vol. 46, no. 1, pp. 420–432, Jan. 2013.
- [44] F. Moschas and S. Stiros, "Dynamic deflections of a stiff footbridge using 100-Hz GNSS and accelerometer data," *J. Surveying Eng.*, vol. 141, no. 4, Nov. 2015, Art. no. 04015003.
- [45] M. Kaloop, J. Hu, and E. Elbeltagi, "Adjustment and assessment of the measurements of low and high sampling frequencies of GPS real-time monitoring of structural movement," *ISPRS Int. J. Geo-Inf.*, vol. 5, no. 12, p. 222, Nov. 2016.
- [46] H. Pehlivan, "Frequency analysis of GPS data for structural health monitoring observations," *Struct. Eng. Mech.*, vol. 66, no. 2, pp. 185–193, 2018.
- [47] F. Moschas and S. Stiros, "Dynamic multipath in structural bridge monitoring: An experimental approach," *GPS Solutions*, vol. 18, no. 2, pp. 209–218, Apr. 2014.
- [48] L. Li and H. Kuhlmann, "Real-time deformation measurements using time series of GPS coordinates processed by Kalman filter with shaping filter," *Surv. Rev.*, vol. 44, no. 326, pp. 189–197, Jul. 2012.
- [49] M. R. Kaloop and D. Kim, "GPS-structural health monitoring of a long span bridge using neural network adaptive filter," *Surv. Rev.*, vol. 46, no. 334, pp. 7–14, Jan. 2014.
- [50] M. R. Kaloop and D. Kim, "De-noising of GPS structural monitoring observation error using wavelet analysis," *Geomatics, Natural Hazards Risk*, vol. 7, no. 2, pp. 804–825, Mar. 2016.
- [51] H.-N. Li, D.-S. Li, L. Ren, T.-H. Yi, Z.-G. Jia, and K.-P. Li, "Structural health monitoring of innovative civil engineering structures in mainland China," *Struct. Monitor. Maintenance*, vol. 3, no. 1, pp. 1–32, Mar. 2016.
- [52] N. Shen, L. Chen, J. Liu, L. Wang, T. Tao, D. Wu, and R. Chen, "A review of global navigation satellite system (GNSS)-based dynamic monitoring technologies for structural health monitoring," *Remote Sens.*, vol. 11, no. 9, p. 1001, Apr. 2019.
- [53] J. Yu, X. Meng, B. Yan, B. Xu, Q. Fan, and Y. Xie, "Global navigation satellite system-based positioning technology for structural health monitoring: A review," *Struct. Control Health Monitor.*, vol. 27, no. 1, p. e2467, Jan. 2020.
- [54] R. D. Adams, D. Walton, J. E. Flitcroft, and D. Short, "Vibration testing as a nondestructive test tool for composite materials," Composite Rel., West Conshohocken, PA, USA, Tech. Rep. ASTM STP 580, 1975, pp. 159–175.
- [55] R. D. Adams, P. Cawley, C. J. Pye, and B. J. Stone, "A vibration technique for non-destructively assessing the integrity of structures," *J. Mech. Eng. Sci.*, vol. 20, no. 2, pp. 93–100, Apr. 1978.
- [56] P. Cawley and R. D. Adams, "The location of defects in structures from measurements of natural frequencies," *J. Strain Anal. Eng. Design*, vol. 14, no. 2, pp. 49–57, Apr. 1979.
- [57] H. Li, J. Ou, X. Zhao, W. Zhou, H. Li, Z. Zhou, and Y. Yang, "Structural health monitoring system for the Shandong Binzhou yellow river highway bridge," *Comput.-Aided Civil Infrastruct. Eng.*, vol. 21, no. 4, pp. 306–317, 2010.
- [58] F. Magalhães, Á. Cunha, and E. Caetano, "Vibration based structural health monitoring of an arch bridge: From automated OMA to damage detection," *Mech. Syst. Signal Process.*, vol. 28, pp. 212–228, Apr. 2012.
- [59] N. M. Apaydın, Y. Kaya, E. Şafak, and H. Alçık, "Vibration characteristics of a suspension bridge under traffic and no traffic conditions," *Earthq. Eng. Struct. Dyn.*, vol. 41, no. 12, pp. 1717–1723, Oct. 2012.

- [60] A. Li, Y. Ding, H. Wang, and T. Guo, "Analysis and assessment of bridge health monitoring mass data—progress in research/development of 'structural health monitoring,'" *Sci. China Technol. Sci.*, vol. 55, no. 8, pp. 2212–2224, Aug. 2012.
- [61] R. Yao and S. N. Pakzad, "Time and frequency domain regression-based stiffness estimation and damage identification," *Struct. Control Health Monit.*, vol. 21, no. 3, pp. 356–380, Mar. 2014.
- [62] M. M. Alamdari, B. Samali, J. Li, H. Kalhori, and S. Mustapha, "Spectral-based damage identification in structures under ambient vibration," *J. Comput. Civil Eng.*, vol. 30, no. 4, Jul. 2016, Art. no. 04015062.
- [63] J. Li, R. Zhang, J. Liu, L. Cao, and Y. F. Chen, "Determination of the natural frequencies of a prestressed cable RC truss floor system," *Measurement*, vol. 122, pp. 582–590, Jul. 2018.
- [64] P. Omenzetter and J. M. W. Brownjohn, "Application of time series analysis for bridge monitoring," *Smart Mater. Struct.*, vol. 15, no. 1, pp. 129–138, Feb. 2006.
- [65] K. Erazo, D. Sen, S. Nagarajaiah, and L. Sun, "Vibration-based structural health monitoring under changing environmental conditions using Kalman filtering," *Mech. Syst. Signal Process.*, vol. 117, pp. 1–15, Feb. 2019.
- [66] T. Kijewski and A. Kareem, "Wavelet transforms for system identification in civil engineering," *Comput.-Aided Civil Infrastruct. Eng.*, vol. 18, no. 5, pp. 339–355, Sep. 2003.
- [67] H. Melhem and H. Kim, "Damage detection in concrete by Fourier and wavelet analyses," *J. Eng. Mech.*, vol. 29, no. 5, pp. 571–577, 2003.
- [68] W. L. Bayissa, N. Haritos, and S. Thelandersson, "Vibration-based structural damage identification using wavelet transform," *Mech. Syst. Signal Process.*, vol. 22, no. 5, pp. 1194–1215, Jul. 2008.
- [69] R. O. Curadelli, J. D. Riera, D. Ambrosini, and M. G. Amani, "Damage detection by means of structural damping identification," *Eng. Struct.*, vol. 30, no. 12, pp. 3497–3504, Dec. 2008.
- [70] W. C. Su, C. S. Huang, C. H. Chen, C. Y. Liu, H. C. Huang, and Q. T. Le, "Identifying the modal parameters of a structure from ambient vibration data via the stationary wavelet packet," *Comput.-Aided Civil Infrastruct. Eng.*, vol. 29, no. 10, pp. 738–757, Nov. 2014.
- [71] S. Baselga, L. García-Asenjo, and P. Garrigues, "Deformation monitoring and the maximum number of stable points method," *Measurement*, vol. 70, pp. 27–35, Jun. 2015.
- [72] C. A. Perez-Ramirez, J. P. Amezcua-Sanchez, H. Adeli, M. Valtierra-Rodriguez, D. Camarena-Martinez, and R. J. Romero-Troncoso, "New methodology for modal parameters identification of smart civil structures using ambient vibrations and synchrosqueezed wavelet transform," *Eng. Appl. Artif. Intell.*, vol. 48, pp. 1–12, Feb. 2016.
- [73] E. Reynders, G. Wursten, and G. D. Roeck, "Output-only structural health monitoring in changing environmental conditions by means of nonlinear system identification," *Struct. Health Monit.*, vol. 13, no. 1, pp. 82–93, 2014.
- [74] S.-S. Jin, S. Cho, and H.-J. Jung, "Adaptive reference updating for vibration-based structural health monitoring under varying environmental conditions," *Comput. Struct.*, vol. 158, pp. 211–224, Oct. 2015.
- [75] J. Chen, Y. L. Xu, and R. C. Zhang, "Modal parameter identification of Tsing Ma suspension bridge under typhoon victor: EMD-HT method," *J. Wind Eng. Ind. Aerodyn.*, vol. 92, no. 10, pp. 805–827, Aug. 2004.
- [76] H. Li, X. Deng, and H. Dai, "Structural damage detection using the combination method of EMD and wavelet analysis," *Mech. Syst. Signal Process.*, vol. 21, no. 1, pp. 298–306, Jan. 2007.
- [77] Y. B. Yang and K. C. Chang, "Extraction of bridge frequencies from the dynamic response of a passing vehicle enhanced by the EMD technique," *J. Sound Vib.*, vol. 322, nos. 4–5, pp. 718–739, May 2009.
- [78] B. Yan and A. Miyamoto, "A comparative study of modal parameter identification based on wavelet and Hilbert–Huang transforms," *Comput.-Aided Civil Infrastruct. Eng.*, vol. 21, no. 1, pp. 9–23, Jan. 2006.
- [79] D. Rezaei and F. Taheri, "Damage identification in beams using empirical mode decomposition," *Struct. Health Monit. Int. J.*, vol. 10, no. 3, pp. 261–274, May 2011.
- [80] N. Roveri and A. Carcaterra, "Damage detection in structures under traveling loads by Hilbert–Huang transform," *Mech. Syst. Signal Process.*, vol. 28, pp. 128–144, Apr. 2012.
- [81] I. Gonzalez and R. Karoumi, "Analysis of the annual variations in the dynamic behavior of a ballasted railway bridge using Hilbert transform," *Eng. Struct.*, vol. 60, pp. 126–132, Feb. 2014.
- [82] B. Chen, S. Zhao, and P. Li, "Application of Hilbert–Huang transform in structural health monitoring: A state-of-the-art review," *Math. Problems Eng.*, vol. 2014, pp. 1–22, Jun. 2014.
- [83] W.-H. Wu, C.-C. Chen, J.-W. Jhou, and G. Lai, "A rapidly convergent empirical mode decomposition method for analyzing the environmental temperature effects on stay cable force," *Comput.-Aided Civil Infrastruct. Eng.*, vol. 33, no. 8, pp. 672–690, Aug. 2018.
- [84] A. Mao, C. G. A. Harrison, and T. H. Dixon, "Noise in GPS coordinate time series," *J. Geophys. Res. Solid Earth*, vol. 104, no. B2, pp. 2797–2816, Feb. 1999.
- [85] W. Jiang, L. Deng, Z. Li, X. Zhou, and H. Liu, "Effects on noise properties of GPS time series caused by higher-order ionospheric corrections," *Adv. Space Res.*, vol. 53, no. 7, pp. 1035–1046, Apr. 2014.
- [86] Y. An, B. F. Spencer, and J. Ou, "A test method for damage diagnosis of suspension bridge suspender cables," *Comput.-Aided Civil Infrastruct. Eng.*, vol. 30, no. 10, pp. 771–784, Oct. 2015.
- [87] J. Bogusz and A. Klos, "On the significance of periodic signals in noise analysis of GPS station coordinates time series," *GPS Solutions*, vol. 20, no. 4, pp. 1–10, 2016.
- [88] J. Xu, S. X. Huang, and F. H. Ma, "The dynamic characteristics analysis for the large bridge based on the improved Hilbert–Huang transformation," *Geomatics Inf. Sci. Wuhan Univ.*, vol. 35, no. 7, pp. 801–805, 2010.
- [89] M. R. Kalooop and H. Li, "Sensitivity and analysis GPS signals based bridge damage using GPS observations and wavelet transform," *Measurement*, vol. 44, no. 5, pp. 927–937, Jun. 2011.
- [90] M. R. Kalooop, E. Elbeltagi, and M. T. Elnabwy, "Bridge monitoring with wavelet principal component and spectrum analysis based on GPS measurements: Case study of the Mansoura bridge in Egypt," *J. Perform. Constructed Facilities*, vol. 29, no. 3, Jun. 2015, Art. no. 04014071.
- [91] J. Xin, J. Zhou, S. Yang, X. Li, and Y. Wang, "Bridge structure deformation prediction based on GNSS data using Kalman-ARIMA-GARCH model," *Sensors*, vol. 18, no. 1, p. 298, Jan. 2018.
- [92] Y. Niu and C. Xiong, "Analysis of the dynamic characteristics of a suspension bridge based on RTK-GNSS measurement combining EEMD and a wavelet packet technique," *Meas. Sci. Technol.*, vol. 29, no. 8, Aug. 2018, Art. no. 085103.
- [93] R. Rao, C. Li, Y. Huang, X. Zhen, and L. Wu, "Method for structural frequency extraction from GNSS displacement monitoring signals," *J. Test. Eval.*, vol. 47, no. 3, May 2019, Art. no. 20180087, doi: [10.1520/JTE20180087](https://doi.org/10.1520/JTE20180087).
- [94] S. X. Huang, X. P. Wang, C. F. Li, and C. Kang, "Data decomposition method combining permutation entropy, spectral substitution with EEMD," *Measurement*, vol. 139, pp. 438–453, 2019.
- [95] R. Benzi, A. Sutera, and A. Vulpiani, "The mechanism of stochastic resonance," *J. Phys. A, Math. Gen.*, vol. 14, no. 11, pp. 453–457, 1981.
- [96] S. Maitam and B. Kosko, "Adaptive stochastic resonance," *Proc. IEEE*, vol. 86, no. 11, pp. 2152–2183, Nov. 1998.
- [97] J. Tan, X. Chen, J. Wang, H. Chen, H. Cao, Y. Zi, and Z. He, "Study of frequency-shifted and re-scaling stochastic resonance and its application to fault diagnosis," *Mech. Syst. Signal Process.*, vol. 23, no. 3, pp. 811–822, Apr. 2009.
- [98] S. Lu, Q. He, and F. Kong, "Note: On-line weak signal detection via adaptive stochastic resonance," *Rev. Sci. Instrum.*, vol. 85, no. 6, Jun. 2014, Art. no. 066111.
- [99] S. Lu, Q. He, D. Dai, and F. Kong, "Periodic fault signal enhancement in rotating machine vibrations via stochastic resonance," *J. Vib. Control*, vol. 22, no. 20, pp. 4227–4246, Dec. 2016.
- [100] X. Liu, H. Liu, J. Yang, G. Litak, G. Cheng, and S. Han, "Improving the bearing fault diagnosis efficiency by the adaptive stochastic resonance in a new nonlinear system," *Mech. Syst. Signal Process.*, vol. 96, pp. 58–76, Nov. 2017.
- [101] Z. Qiao, Y. Lei, J. Lin, and F. Jia, "An adaptive unsaturated bistable stochastic resonance method and its application in mechanical fault diagnosis," *Mech. Syst. Signal Process.*, vol. 84, pp. 731–746, Feb. 2017.
- [102] Y. Lei, Z. Qiao, X. Xu, J. Lin, and S. Niu, "An underdamped stochastic resonance method with stable-state matching for incipient fault diagnosis of rolling element bearings," *Mech. Syst. Signal Process.*, vol. 94, pp. 148–164, Sep. 2017.
- [103] S. Lu, Q. He, and J. Wang, "A review of stochastic resonance in rotating machine fault detection," *Mech. Syst. Signal Process.*, vol. 116, pp. 230–260, Feb. 2019.
- [104] A. Narayanan and M. Moore, "Quantum-inspired genetic algorithms," in *Proc. IEEE Int. Conf. Evol. Comput.*, May 1996, pp. 61–66.

[105] K. Han and J. H. Kim, "Genetic quantum algorithm and its application to combinatorial optimization problem," in *Proc. Congr. Evol. Comput.*, Jul. 2000, pp. 1354–1360.

[106] L. Wang, F. Tang, and H. Wu, "Hybrid genetic algorithm based on quantum computing for numerical optimization and parameter estimation," *Appl. Math. Comput.*, vol. 171, no. 2, pp. 1141–1156, Dec. 2005.

[107] S. Zhao, G. Xu, T. Tao, and L. Liang, "Real-coded chaotic quantum-inspired genetic algorithm for training of fuzzy neural networks," *Comput. Math. Appl.*, vol. 57, nos. 11–12, pp. 2009–2015, Jun. 2009.

[108] Y. M. Huang and M. Lin, "A method based on heterodyne stochastic resonance to detect vortex shedding frequency," *Chin. J. Mech. Eng.*, vol. 44, no. 4, pp. 139–142, 2008.

[109] A. Rytter, "Vibrational based inspection of civil engineering structures," Ph.D. dissertation, Dept. Building Technol. Struct. Eng., Aalborg Univ., Aalborg, Denmark, 1993.

[110] P. S. Oliveto and C. Witt, "Improved time complexity analysis of the simple genetic algorithm," *Theor. Comput. Sci.*, vol. 605, pp. 21–41, Nov. 2015.

[111] H. Aytug and G. J. Koehler, "The effect of multiple optima on the simple GA run-time complexity," *Eur. J. Oper. Res.*, vol. 178, no. 1, pp. 27–45, Apr. 2007.

[112] X. Wang, S. Huang, C. Kang, G. Li, and C. Li, "Integration of wavelet denoising and HHT applied to the analysis of bridge dynamic characteristics," *Appl. Sci.*, vol. 10, no. 10, p. 3605, May 2020.



GUANQING LI was born in 1990. He is currently pursuing the Ph.D. degree in geodesy and surveying engineering with Wuhan University, China. His research interests include precise engineering surveying, precise integrated positioning and attitude determination systems, and deformation monitoring.



WEN ZHANG was born in 1988. He received the B.S. degree from Wuhan University, in 2013, where he is currently pursuing the Ph.D. degree. His research interests include precision engineering survey, and deformation monitoring analysis and disaster forecast.



XINPENG WANG was born in 1982. He received the B.S. degree in surveying and mapping engineering from Henan Polytechnic University, in 2006, and the M.S. degree in geodesy and surveying engineering from the Hefei University of Technology, in 2012. He is currently pursuing the Ph.D. degree with Wuhan University. His research interests include precision engineering measurement, deformation monitoring, and disaster early warning.



CHENFENG LI was born in 1990. He received the M.S. degree in geodesy and surveying engineering from Jiangxi Polytechnic University, in 2015. He is currently pursuing the Ph.D. degree in geodesy and surveying engineering with Wuhan University, China. His research interests include crustal deformation and precise integrated positioning.



SHENGXIANG HUANG was born in 1964. He received the B.S. degree from the Wuhan Technical University of Surveying and Mapping, in 1986, the M.S. degree, in 1993, and the Ph.D. degree, in 2001. He has been a Professor with Wuhan University, since 2000. His research interests include deformation monitoring and disaster early warning, GNSS geoscience application, and precision engineering measurement.



YARONG WANG was born in 1994. He received the B.S. degree in surveying and mapping engineering from Central South University, in 2017. He is currently pursuing the M.S. degree with Wuhan University. His research interests include deformation monitoring and disaster early warning.

...